Content Available online at: www.bpasjournals.com

A CONTENT BASED MEDICAL IMAGE RETRIEVAL WITH HYBRID FEATURE EXTRACTION AND DEEP LEARNING MODEL FOR BRAIN TUMOR CLASSIFICATION

[1*]M.Arthi, [2]Dr.V.P.Eswaramurthy
[1*]Research Scholar, Department of Computer Science, Periyar University
Salem-636011.
Email: arthykvarshana@gmail.com
[2]Assistant Professor of Computer Science, Government Ars and Science College,
Komarapalayam 638183
Email: eswaramurthy@yahoo.com

Abstract: When detected early, brain tumors (BT) are also frequently treatable conditions. The accuracy with which the abnormality in the query image is recognized and determines the diagnosis of the condition. Utilizing a combination of Feature Extraction (FE) and Similarity Matching (SM) techniques, computer-aided automated systems like Content-Based Medical Image Retrieval (CBIR) approach are used to retrieve Query-Based (QB) images from a huge database. For the BT to be effectively treated, an accurate diagnosis is essential. In order to help the radiologist diagnose the BT, this work suggests an intelligent CBIR system that recovers similar pathology carrying Magnetic Resonance Images (MRI) of the brain from a medical database. Since images within the same disease class differ in terms of severity, density, and other features, a single Feature Vector (FV) will not be very effective in identifying similar images in the medical domain. A two-level hierarchical CBMIR system was suggested in this study for addressing this issue. It finds the most similar images in the specified class after first classifying the Query Image (QI) of a BT as benign or malignant. During the image preprocessing step, image Normalization, and Noise Reduction (NR) is carried out. After this step, the image segmentation using WatersShed (WS) method is employed for the identification of the tumor part in MRI image and FE using Hybrid Fuzzy (HF) Dove Swarm Optimization Algorithm (DSOA). Then the Feature Selection (FS) is performed by making use of the modified BAT (mBAT) algorithm. At last, an effective method for BT diagnosis is suggested a Convolutional Neural Network (NN) (CNN). Brain MRI data from a Medical imaging (MI) database have been used in experiments. By increasing precision, recall, and retrieval time, the suggested method produces effective retrieval outcomes.

Keywords: Content-Based Image Retrieval (CBIR) system, preprocessing, WaterShed (WS) method, hybrid fuzzy Dove Swarm Optimization (HF-DSO), modified BAT (mBAT) algorithm and Convolutional Neural Network (CNN).

1. Introduction

Anatomical (structure) and physiologic (functional) data about patients at the organ and tissue levels has typically been the main focus of MI. This emphasis has provided significant benefits in the identification and diagnosis of human illness and injury by fostering the connection of imaging results with pathological situations [1]. Wilhelm Conrad Roentgen's

discovery of the X-ray in 1895 marked the beginning of MI. Nuclear medicine, which combined radionuclides and radiopharmaceuticals, was made possible later in 1950. Following that, the principles of sonar were used to develop diagnostic imaging, and in the 1960s, UltraSound (US) was developed. Because it has no negative biological consequences, US has grown to be a very popular imaging tool. Radiation, Digital Imaging (DI) and Communications in medicine (DICOM), MRI, Computer Tomography (CT) images, and Picture Archiving and Communication System (PACS) were among the MI techniques that were subsequently employed in the field [2]. PACS, which enables image retrieval, storage, distribution, and presentation, came along with the revolution in DI. The DICOM standard, which includes a network communication protocol, is used to store and transmit data related to MI.

A large database was created as a result of the digital medical imaging technology's quick adoption in hospitals, which produced a lot of images daily [3]. In order to manage such a large database, the goal of Image Retrieval (IR) is to offer an efficient method. The main goal of IR is to identify images that match the QI.For IR, Several Text-based (TB) techniques, termed CBIR were presented [4]. However, the text is laborious and the TB Retrieval (TBR) was quite prone to errors. To solve these problems with TBR, CBIR also known as Query By Image Content (QBIC) or Content-Based Visual IR (CBVIR) was subsequently created.

Colour, texture, shape, size, intensity, location, and other visual aspects of an image form the basis of CBIR systems. Using these visual aspects, variety of Visual-Based Retrieval (VBR) techniques have been developed [5]. In computer-aided diagnostics (CAD), CBMIR is today recognized as an essential medical tool that aids doctors in the detection and treatment of numerous diseases.

Doctors can better understand a patient's disease or injury status and help them understand his/ her medical report by using CBMIR to retrieve similar images and case histories. Additionally, it facilitates more accurate report preparation for the radiologist regarding a specific diagnosis. CBMIR also assists in teaching and research besides from the diagnostics .
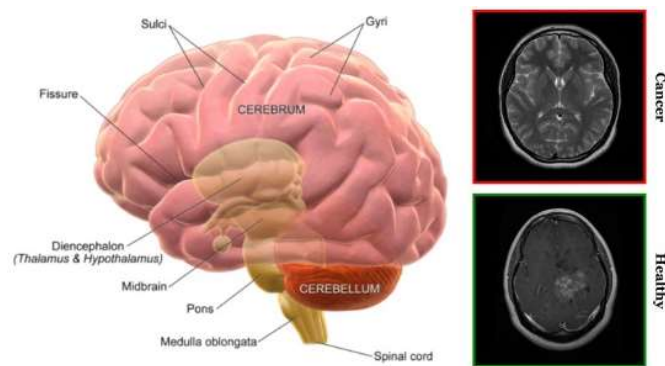
Fig. 1   The human brain structures

Globally, the mortality rate raises due to the occurrence of Cancer. Early cancer detection can assist save death and that it is not practical and it is stated by World Health Organization (WHO) [6]. A growth might be malignant, precancerous, or benign, unlike cancer. The fact that benign tumors do not spread to other tissues and organs sets them apart from malignant tumors. In surgery, doctors are frequently able to remove them. The most

popular method for this kind of differential medicinal growth is MRI [7]. But for early tumor diagnosis, radiologists' expertise is crucial. It is necessary to classify the nature of tumor tissue as normal or cancerous, the diagnostic procedure will not be performed. A dependable and effective medical tool or technique for tumor development subdivision and MRI (IC) Image Classification is extremely important in today's world of constant innovation and new technologies.

In order to ensure early BTclassification and detection, a system must be developed [8]. When classifying tumors, classification systems should provide high levels of accuracy because wrong classification might lead to adverse effects. Machine Learning (ML) methods and algorithms used for detection and classification usually require an appropriate algorithmic approach on the data to attain greater accuracy. The maximum algorithmic accuracy is attained via applying the appropriate classification algorithm to data. To classify the tumor class, certain parameters are required. Since these factors depend on one other for classification, they are then combined [9]. MRI and CT scans are used in laboratories on a daily basis to diagnose a range of tumor patients, and the features of the tumors are also recorded as patient data. Then, this data can be utilized for other patients' analysis and prediction. To identify and predict the type of tumor with the support of ML. The development of new techniques for health care-related challenges can be facilitated by computer-based technologies, which can aid radiologists [10], neurologists, and neurosurgeons in their tasks.

Applications involving speech, biomedical signals, or medical images benefit greatly from Deep Learning (DL). The Deep CNN (DCNN) structures, which enables excellent self-learning, is now more advanced, reducing the need for handcrafted features. For enhancing the accuracy of classification of tumors from brain MRI, it is imperative to create sophisticated algorithms for automatic and quick BT identification [11].

To train a DCNN, huge datasets of MI are required. Some of the challenging application-related problems include choosing the right DCNN architectures, fixing overfitting and convergence problems, and optimizing learning parameters and HyperParameters (HP) for best results. Utilizing a combination of FE and SM techniques, computer-aided automated systems like CBMIR approach are used to retrieve QB images from a huge database. For the BT to be effectively treated, an accurate diagnosis is essential.

In order to help the radiologist diagnose the brain tumor, this work suggests an intelligent CBIR system that recovers similar pathology carrying MRI of the brain from a medical database. Since images within the same disease class differ in terms of severity, density, and other characteristics, a single FV will not be very effective in discovering similar images in the medical realm. To resolve this issue, this study recommends a two-level hierarchical CBMIR system that finds the most similar images within the designated class after first classifying the QI of a BT as benign or malignant.

The remainder of the study is organized as follows: Section 2 examines some of the most recent methods for detecting BT utilizing DL and ML approaches. The suggested methodology's approach is presented in section 3. Section 4 contains the results and a discussion. Future work and the conclusion are covered in section 5.

2. Literature Review

BT fall into the category of swiftly deadly disease that affect many people. To verify early tumor detection and classification, tumor organization and detection are crucial. The

classification and segmentation procedures are used because incorrect identification leads to dreadful and fatal outcomes. This section examines a few new technologies that use various ML algorithms to detect BT.

Using a pre-trained GoogLeNet, a Deep (TL)Transfer Learning (DTL) method for FE from brain MRI images was suggested by Deepak et al. [12]. The FE are classified by the integration of proven classifier models. A MRI dataset from figshare is used in the experiment to administer a five-fold (CV) Cross-Validation procedure at the patient level. With a mean classification accuracy of 98%, the suggested approach exceeds all standard methods. F-score, specificity, accuracy, recall, and Area Under the Curve (AUC) were also included in the study as performance metrics. This research also tackles a real-world issue by evaluating the system with less training data. The study's findings suggest that when there is a shortage of MI, and TL is considered to be an effective method.

For content-based CT IR and define medical CT images, a new image feature definition based on the Local Wavelet (LW) Pattern (LWP) was introduced by Dubey et al. [13]. By utilizing the correlation among the center pixel (CP) and the local neighboring data, the LWP for each pixel in the CT image has been determined by suggested method. The proposed method leverages the link among the nearby pixels first, then considers its relationship with the CP, by using LW Decomposition (LWD). Compared to this, the local binary pattern simply considers the relation between a CP and its surrounding pixels. This paper is novel in the following twoaspects: 1) LWD is used to encode local neighboring data; 2) LWD values and altered center pixel values are used to compute LWP. Then evaluating the precision and recall of the technique using three CT image databases. The simulation outcomes indicate that the recommended method execute well for CT IR than other methods when compare it to other SOTA local image descriptors.

By using CNN, pre-trained models, and the Manta Ray Foraging Optimization (MRFO) algorithm on X-ray and MRI to detect BT patients with great accuracy and efficiency, the system suggested was discussed by Aljohani et al. [14]. Furthermore, MRFO will be used to adjust the CNN and TL HP, improving the pre-trained model's performance. To create the models, Kaggle provided two public datasets. The 2 X-ray classed are contained in first dataset, whereas the second dataset consists of three (CE) contrast-enhanced T1-weighted MRI classes. An initial diagnosis of "Healthy" (or "Tumor") should be made for the patient. The patient's brain is considered "healthy" if there are no abnormalities in the brain and the scan provides this outcome. An MRI will be done on the patient if a scan indicates that they have a tumor. Next, the tumor type (glioma, pituitary, and meningioma) will be determined using the 2nd suggested classifier.

Three forms of BT like glioma, meningioma, and pituitary tumor are classified using an EfficientNetB3 pre-trained model, which was presented by Balamurugan et al. [15]. To find the BT, the pre-trained EfficientNetB3 version's features are first utilized to identify several EfficientNet modules. Every method is evaluated using three different kinds of BT datasets. The concatenated functionalities of EfficientNetB3 and Genetic Algorithms (GA) provide superior accuracy than the current DL frameworks. Apart from using Tensor Flow 2, another technique used to enhance and promote the model training process is Nesterov-accelerated adaptive moment estimation (Nadam). 99.56% accuracy, 98.9% sensitivity, 98.6% specificity, 98.9% F-score, 98.9% precision, and 99.54% recall are achieved using the suggested CNN

approach.

A DCNN model was introduced by Gómez-Guzmán et al. [16] for the purpose of classifying BT. 6 pre-trained CNN frameworks are examined and a generic CNN model is put into practice. The Msoud dataset is made up of 7023 MRI scans that were taken from the Br35H, SARTAJ, and Fighshare datasets. The MRI in the dataset represents four classes: glioma, meningioma, and pituitary are among the BT classes, while one class comprises healthy brains. The input MRI images are employed for the model training and it is subjected to many preprocessing techniques in this work. The CNN frameworks that were assessed with EfficientNetB0, ResNet50, InceptionV3, InceptionResNetV2, Xception, MobileNetV2, and Generic CNN.

The study concluded that InceptionV3, with an average accuracy of 97.12%, was the best CNN model for the dataset after comparing all models, including a generic CNN and six pre-trained models. Doctors who specialize in BT (ED) Early Detection may benefit from the development of these procedures.

In order to classify the BT types, Rasheed et al. [17] presented a unique CNN method. The pre-trained VGG16, VGG19, ResNet50, MobileNetV2, and InceptionV3 procedures that have been previously published in the literature were contrasted with the algorithm through testing on benchmarked data. High classification accuracy of 98.04%, precision, recall, and f1-score success rate of 98% were all shown by the research's outcomes. The classification results demonstrated that a high degree of accuracy may be achieved in classifying the most prevalent types of BT. The suggested approach can help physicians diagnose BT more quickly and accurately because of its strong generalization ability and quick execution rate.

In order to identify BT classifications based on MRI data, AlTahhan et al. [18] introduced hybrid CNN. 2880 T1-weighted, CE MRI brain images are utilized as the dataset. Gliomas, meningiomas, and pituitary tumors, class of no tumors are the 3 primary types of BT found in the dataset. First, for the classification procedure, 2 pre-trained, fine-tuned CNN, GoogleNet and AlexNet were employed. Their respective validation and classification accuracy was 91.5% and 90.21%. Next, 2 hybrid networks (AlexNet-SVM and AlexNet-KNN) were used to enhance the fine-tuning of AlexNet's performance. The validation and accuracy of these hybrid networks were 96.9% and 98.6%. Following the export of these networks, a particular dataset was used for testing, and the results showed that the fine-tuned versions of GoogleNet, AlexNet, AlexNet-SVM, and AlexNet-KNN produced accuracy values of 88%, 85%, 95%, and 97%. The suggested approach would speed up the clinical diagnosis process by automatically identifying and classifying BT using MRI scans.

In order to classify BT into 3 categories based on their T1-weighted CE-MRI images, Wu et al. [19] presented an ensemble of pre-trained CNN. Three pre-trained CNNs (Inception-v3, Resnet101, Densenet201) that showed the best classification performance (i.e., accuracy of 96.21%, 97.00%, and 96.54%,) on the CE-MRI benchmark dataset were selected to serve as the basis for the ensemble model. The elements that the ensemble model's backbone networks had further extracted were recognized by a Support Vector Machine (SVM).

DL is an artificial technique suggested by Muhammad et al. [20] that is used to create systems or models that can learn meaningful features from the dataset or train themselves automatically. In order to create the classification models of the BT using the MRI image dataset, this technique has been used in this work. Each model was assessed using measures

for accuracy, sensitivity, specificity, and area under the ROC curve. The models were developed using the DL algorithms VGG16 and ResNet50. In terms of correctly classifying malignant cases with 94.30% accuracy and classifying BT as benign or malignant with 96% accuracy, the VGG16 classification model has done relatively better than the ResNet50 model. With 93.10% accuracy, ResNet50 has surpassed the VGG16 classification model in the capacity to accurately diagnose benign cases of BT. However, with 91.20% accuracy, the model created using the ResNet50 DL algorithm performed better than the VGG16 classification model in terms of how well it distinguishes between malignant and benign cases.

Using three publicly accessible datasets and MRI, Gull et al. [21] created a multistage classification system. 3 datasets: the first from the Kaggle Repository (Dataset-1), the second from Figshare (Dataset-2), and the third from REMBRANDT (Dataset-3) are used to classify MR images into various grades. Several augmentation methods are used to expand the MR image data size. The suggested models removed noise during pre-processing by achieving a higher (PSNR) Peak Signal-to-Noise ratio.

Classification-1 is the first suggested deep CNN framework that was able to classify MR images into 2 categories: (i) normal and (ii) abnormal, with an accuracy rate of 99.40%. In contrast, Classification-2, achieved 97.78% accuracy in classifying BT into 3 distinct types: meningioma, glioma, and pituitary and it is attained by employing the secondly suggested CNN framework.

Based on CNN, which are reinforced by a multi-branch network that is improved with an inception block, serves as the suggested BT classification model by Rastogi et al. [22]. This model effectively uses a five-fold CV method. The Br35H dataset includes 826 photos with gliomas, 822 images with meningiomas, 827 images with pituitary tumors, and 395 images without any malignancies, was used to carefully calibrate and assess this all-inclusive method. This research carefully focuses on differentiating between 3 types of tumors, as well as cases in which there are no tumors. The Gaussian Naive Bayes (GNB), Logistic Regression (LR), Decision Tree (DT) Classifier, and Support Vector Classifier (SVC) are a range of SOTA classification models that are employed, the outcomes are meticulously compared the above models to suggested model.

3. Proposed Methodology

In order to find the most similar photos within the selected class, this research effort suggests a two level hierarchical CBMIR system that first classifies the QI of a BT as benign or malignant. During the image preprocessing step, image Normalization, and noise reduction is carried out. After this step, the image segmentation using watershed method is employed for the identification of the tumor part in MRI image and feature extraction using hybrid fuzzy dove swarm optimization algorithm. Then the feature selection is performed by making use of the modified BAT (mBAT) algorithm. Finally the CNN is proposed for the diagnosing the brain tumor in an efficient manner.
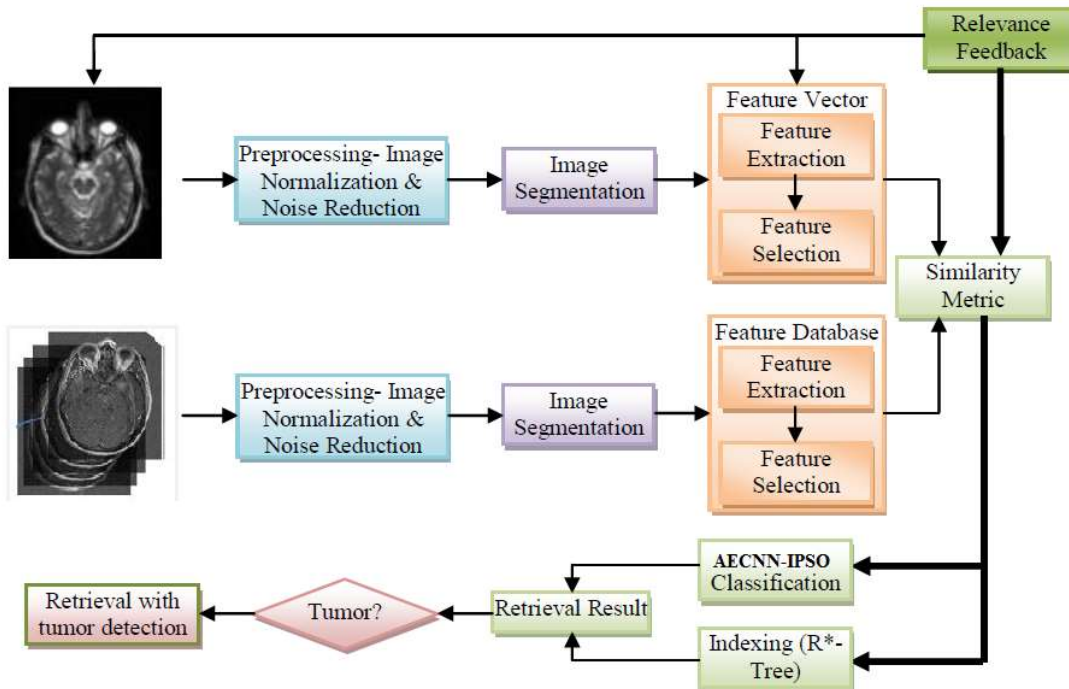
Fig. 2 **The procedure of the suggested approach**

3.1. Preprocessing

De-noising, or removing unnecessary noise from photos, is the process known as preprocessing. One kind of preprocessing that blurs images smoothly without affecting boundaries is called smoothing [23]. While the dataset used for this procedure was taken from a website that might have noise in it, current MRI technology has the potential to provide more accurate images. Noises can affect the images that are transmitted through electronic sources. Following normalization to achieve consistency in intensity/gray level, the MRI images are rejected illumination in this preprocessing stage. In order to either improve or alter the image, the improved median filter is then used for image filtration.

(a) Image Normalization

A major problem in face recognition is illumination variation. Non-uniform contrast, or an uneven distribution of intensity/Gray Levels (GL), is a feature of images with uncontrolled lighting. The Histogram Equalization (HE) technique is used to achieve equality in these levels [24].

It is possible to find the pixels equalization value (h) over L gray levels with given a $M \times N$ image by using the Weibull Cumulative Distribution Function (WCDF) at each Pixel Value (V).

Next, using the HE specified by the following formula, the distribution of the pixel intensity values in the image I(x,y) is changed into a uniform distribution on interval [0,1]. Mathematically, for a GL of k, k = 0, 1, ⋯, L-1.

$$h(z) = \left(\frac{WCDF(V) - MINWCDF}{MXN - MINWCDF} \right)(L - 1) \tag{1}$$

(b) Image De-noising using Filtering

Due to variations in illumination, images frequently exhibit Gaussian Noise (GN) by default. Pixel-Based Filtering (PBF) techniques are employed to de-noise it. The Images in this

experiment are enhanced using the Enhanced MF. The Euclidean Distance (ED), which is almost used as a cutoff value, is another tool used by this algorithm to measure the "smoothness" of the working window (WW). This value is used for fine-tuning the algorithm for detecting noise. The following additional variables are being defined:

zavg=mean gray level value in region Sxy

eucavg=average euclidean distance in region Sxy

cutoff=limit the euclidean distance in Sxy

The following pseudo-code describes the algorithm:

```
compute z_avg for the WW
compute ED among z_avg and
all other pixels in the WW
compute average ED for this
WW as euc_avg
if euc_avg > cutoff:
return z_med
else:
increase window_size
if window_size <= S_max:
continue
else:
return z_xy
```

The pixel data that deviates from a pre-established norm is interpreted by the block-wise algorithm as coming from a noise signal. Since MF with local statistics is shown to be effective in controlling grainy-patterned speckle noise, the value of the working window's CP is replaced in this case by the WW median intensity value [13].

Finally, the result of preprocessing method is shown in Fig.2 (b) along with for the input MRI image Fig.2 (a).

3.2. Image Segmentation using watershed algorithm

One gradient-based segmentation technique is called WaterShed Segmentation (WSS). It considers the image's gradient map to be a relief map. Like a dam, it segments the image. Catchment basins are the names given to the segmented areas. Many image segmentation issues are resolved by WSS. For images with a higher intensity value, it is preferred. Oversegmentation is the root cause of WSS. Marker controlled WSS is employed to control over segmentation. Edge detection (ED) is an effective application for the Sobel operator. The edge of the object is distinguished in marker controlled WSS using the Sobel operator.

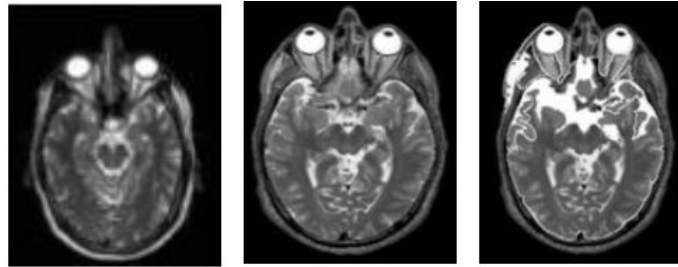The following are the sobel masks in matrix form:

$$M_X = \begin{bmatrix} -1 & -2 & -1 \\ 0 & 0 & 0 \\ 1 & 2 & 1 \end{bmatrix}, \quad M_Y = \begin{bmatrix} -1 & 0 & 1 \\ -2 & 0 & 0 \\ -1 & 0 & 2 \end{bmatrix} \tag{2}$$

In marker-controlled WSS, the Gradient Magnitude (GM) equation is

$$M = \sqrt{M_X{}^2 + M_Y{}^2} \tag{3}$$

$$Angle, \theta = \tan^{-1}\frac{M_Y}{M_X} \tag{4}$$

Fig. 3   **(a) Input MRI (b) Image Preprocessing Result (C) Object boundaries by applying watershed transform.**

3.3. Feature Extraction using hybrid fuzzy DSOA

Applying fuzzy set theory for the adaptive adjustment of DSO acceleration coefficients, this will helps in enhancing the accuracy and efficiency of search activities and the above mentioned will be considered as the benefits of suggested FPSO.

3.3.1. Fuzzy Logic (FL) system

An expansion of the well-known Binary Logic (BL) is FL. In contrast to binary-valued logic, which only handles Binary Values (BV) of 0 or 1, FL is a multivalued logic. For this reason, FL is thought to include BL as a particular case [24]. FL also imitates how events are represented in a human-like manner. In BL, a temperature is considered hot if it exceeds a given predictable value and cool if it falls below it. In FL, on the contrary, linguistic notations like extremely hot, hot, normal, cold, and very cold can be used to express the temperature variable.

In a fuzzy system, the output is usually produced through a sequential process involving fuzzification, the inference system, and defuzzification. The crisp value of the input variable is changed to a fuzzy value by the first procedure, fuzzification. Fuzzy membership functions (FMF), which indicate each variable's degree of belonging to these MFs, are used to represent each input or output variable. The rule-based system is the core component of the inference system. Each rule represents a solution to a particular situation and is expressed in the IF (antecedent) THEN (consequent) form.

Typically, a process control expert assists in the development of these rules. Fuzzy conditional statements can be expressed simply and directly as follows:

THEN output is MF2, and IF input is MF1.

Here, linguistic values MF1 and MF2 are defined by FMF on universes of the discourse of the input and output. Fuzzy Rules (FR) can be formulated in two different ways: The rules of Takagi-Sugeno-Kang (TSK). The following is an example of a Mamdani-type FR-based two-input, single-output model:

THEN seems to be large, as both 1 and 2 in IF is small.

Here, the values for the inputs are in1 and in2, and the output is out. The form of a Sugeno-type fuzzy rule in a two-input, single-output model is as follows:

Out = f (in1, in2) IF in1 = MF1 and in2 = MF2.

Here, a linear (L) or nonlinear (NL) function of the input variables in1 and in2 are represented as f(in1, in2).The FMF in the IF can be represented as MF1 and MF2. Then, a crisp function in THEN is represented as out = f(x, y).

The logical combination of the inputs for the fuzzy variables is the IF of both types. On the other hand, the output of the Mamdani-type rule is indicated by a fuzzy variable, but in the

TSK-type, the output is represented by a L/NL equation. Usually, the "Min" operator yields the output for each rule. The aggregate of all firing rules, or the logical total of these rules (the "Max" operator), provides the final fuzzy output. Defuzzification is the last step that yields the final, crisp result.

3.3.2. Dove Swarm Optimization (DSO)

Doves search for crumbs in plazas where there are crumbs present and It is easy to notice that. Not all doves may be satisfied, but some may be satisfied. Doves can be seen flying forward to locations in search of additional crumbs if they are unsatisfied [25]. The fed doves' ability to occupy areas with the majority of crumbs becomes apparent over time. A novel optimal algorithm that is inspired by doves' foraging behavior has been proposed by others. $f(W)$ is the optimization (OF) Objective Function in this method. Within a dataset, each data pattern, W, is recognized as a location that has crumbs, and overall crumbs at that location represented by $f(W)$. The most effective solution is the location that features the highest number of crumbs.
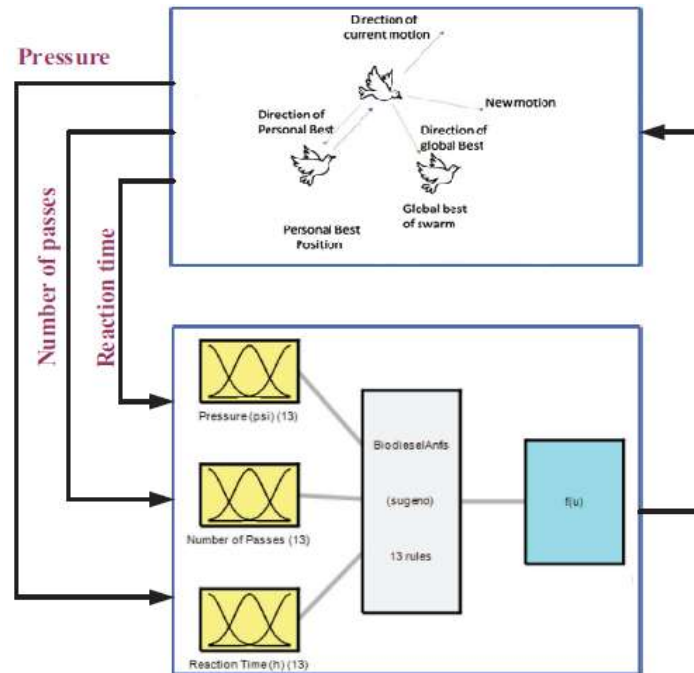

Fig. 4   The procedure of FDSO

Step1: Dove count has been determined and in a solution space, these doves are placed. Let N be the predetermined number of doves. It is recommended to distribute them uniformly across a rectangular space, While the doves can be positioned in a variety of random patterns throughout the space.

Step2: For the dove $d, d = 1, \ldots \ldots N$. Then, s_d^e, and $e = 0$ are fixed. Here, the degree of satiety is denoted as s_d^e, and the epochs is denoted as e. There are two methods for initializing the PV $W_d \subset R^M$ of the d. Initializing W_d at random around the solution space is the simplest method. Initializing the lattice initialized technique provides an alternative. The following stages is shown: To expedite the process of training in order to create a topologically ordered (FM) Feature Map, two effective weight initialization strategies were put forth. Provide an initialization strategy that is particularly appropriate for the algorithm based on the

initialization methodology.

Assume that the parameter space's smallest hyper-rectangle is $[l_1, u_1] \ldots \ldots [l_M, u_M]$. It includes all of the parameters' valid values.

In a- dimension solution space, up bound can be denoted as *ua*. Similarly, the low bound in a- dimension solution space is denoted as *la*. The n-dimensional hyper-rectangle can be compressed into a 2-D plane, thereby allowing a 2-D grid to effectively cover the SS, and it is considered to be the essential idea of the suggested initialization method. Then, to index the rectangular rectangular cells from 1 to A×B, they employ i and j. The following are the specific steps:

Step 2-1. Cell initialization on the 4 borders: The four neurons located at the network's corners have initialized their weight vectors to (5&6).

$$\underline{w}_{1,1} = (l_1, l_2, \ldots \ldots l_M)^T \tag{5}$$

$$\underline{w}_{A,B} = (u_1, u_2, \ldots \ldots u_M)^T \tag{6}$$

$$\underline{w}_{1,B} = (l_1, l_2, \ldots \ldots l_{\lfloor \frac{M}{2} \rfloor}, u_{\lfloor \frac{M}{2} \rfloor} + 1, \ldots u_M)^T \tag{7}$$

$$\underline{w}_{A,1} = (u_1, u_2, \ldots \ldots u_{\lfloor \frac{M}{2} \rfloor}, l_{\lfloor \frac{M}{2} \rfloor} + 1, \ldots l_M)^T \tag{8}$$

Step 2-2. Cell Initialization on the 4 boundaries: According to (9), initializing the starting values of the cells on the four boundaries.

$$\underline{w}_{1,j} = \frac{\underline{w}_{1,B} - \underline{w}_{1,1}}{B-1}(j-1) + \underline{w}_{1,1} = \frac{j-1}{B-1}\underline{w}_{1,B} + \frac{B-j}{B-1}\underline{w}_{1,1} \quad for \ j \tag{9}$$
$$= 2, \ldots ., B-1$$

Step 2-3. Remaining cell initialization: All four of the network's corners have initialized weight vectors. From left to right and top to bottom, initialize the remaining neurons. After selecting several sizes, then assess the outcome. The training outcome is then evaluated by counting the winner numbers of every neuron and the difference value.

The following represents the learning rate's decrease rate from its initial value of 0.1.

$$\eta(n) = \eta_0 \times \left(1 - \frac{t}{T}\right) = 0.1\left(1 - \frac{t}{100}\right) \tag{10}$$

Here, η_0 denotes the initial learning rate. The iterative number can be denoted as t.

Step3: Determine the total number of crumbs at the location of the *dth* dove at each epoch by computing the (FF) fitness function $f\left(w_j^e\right), j = 1, \ldots N$ for all doves.

Step4: Find the dove d_j^e that is closest to the maximum number of crumbs at epoch e using a maximum criterion:

$$d_j^e = \arg\max\{f(w_j^e)\}, \quad for \quad j = 1, \ldots, N \tag{11}$$

Step5: By the following equation, the degree of satiety for every dove can be updated.

$$S_j^e = \lambda S_j^{e-1} + e^{\left(f(w_j) - f(w_{df})\right)}, \quad for \ j = 1, \ldots, N \tag{12}$$

Step6: The maximum criterion was applied for selecting d_s^e

$$d_s^e = arg \max_{1 \le j \le N}\{S_j^e\}, \quad for \ j = 1, \ldots, N \tag{13}$$

d that has the best foraging performance, ds, was chosen by (12) making it the one that other doves in the flock ought to imitate.

Step7: Utilizing the following maximum criterion, update the position vector (PV) of each dove:

$$w_j^{e+1} = w_j^e + \eta \beta_j^e \left(w_{ds}^e - w_j^e \right) \tag{14}$$

Here,

$$\beta_j^e = \left(\frac{S_{bs}^e - S_j^e}{S_{bs}^e} \right) \left(1 - \frac{\left\| w_j^e - w_{ds}^e \right\|}{maxDistance} \right) \tag{15}$$

$$maxDistance: \max_{1 \le j \le N} \left\| w_j - w_j \right\| \tag{16}$$

For updating the PV of d, the parameters, η, represent the learning rate. The updating equations (14)–(16) are listed as follows.

Step8: Proceed to step 3.

Until the terminate condition is satisfied, raise the epochs count by one (i.e., $e = e+1$). It is expressed as.

$$|f_{ds}^e - T(e)| \le \varepsilon \, ore \le the \, set \, \max epoch \tag{17}$$

The order of complexity of the DSOA is represented as $O \, (NNd \, e)$.

Here, number of doves can be denoted as $N. \, e$ denotes the epochs count, and the number of data points in the dataset can be denoted as $Nd.$

The best solution to find the minimum (w_j^e), when the optimization is the minimum criterion. Therefore, it is possible to alter (11) and (12) to (18) and (19), respectively.

$$d_j^e = arg \, \min\{f(w_j^e)\}, \qquad for \, j = 1, \dots, N \tag{18}$$

$$S_j^e = \begin{cases} \lambda S_j^{e-1} + e^{\left(f(w_j) - f(w_{df}) \right)}, & if \, f(w_{df}) \ne 0 \\ \lambda S_j^{e-1} + 1, & if \, f(w_{df}) = 0 \\ \qquad for \, j = 1, \dots \dots, N \end{cases} \tag{19}$$

The updating rules provided in Equations (8)–(10) and it is interpreted as follows for ease of understanding:

1. Emulating the conduct of the best individual in the flock and it was attempted by an individual, after being affected by their success. In order to get more food, doves will gravitate toward the dove that is the sattiest. The PV *wej* is updated to more closely resemble the PV of the d with the d_s^e, w_{ds}^e. $\left(i.e., w_j^{e+1} = w_j^e + \eta \beta_j^e \left(w_{ds}^e - w_j^e \right) \right)$, in order to imitate this social learning.

2. A dove is more likely to become conservative and hesitant to alter its current foraging strategy when it is at a higher level of satiety. On the other hand, a dove that is less sated would likely be more inclined to mimic the actions of the best individual and have a strong urge to alter its current foraging strategy. By proportionally altering the first term value on the RHS of (9), this social impact is simulated.

$$(i.e., \left(\frac{S_{bs}^e - S_j^e}{S_{bs}^e} \right))$$

3. The social impact is inversely related to the distance among d and the best d in the flock since, in short, social impact diminishes with distance. By setting the adjustment amount proportionate to the value of the 3rd term on the RHS of (16) (i.e., $(1 - \frac{\left\| w_j^e - w_{ds}^e \right\|}{maxDistance})$)), one can replicate this type of social impact.

3.4. Feature Selection using Improved Bat Algorithm (IBA)

Despite BA implementation demonstrating its effectiveness, when it comes to

exploration, the Bat has many shortcomings [18]. Thus, on the majority of multimodal test functions, it is easily caught in the local minimum. Velocity update adjustments are used to enhance the exploration and exploitation capabilities of BA to solve this problem with typical BA.

A. Initialization of Bat Population

Using real-valued vectors of dimension d and number of bat n, an initial population is randomly created while taking lower and higher bounds into account.

$$x_{ij} = x_{\min j} + rand(0,1)(x_{\max j} - x_{\min j}) \tag{20}$$

In dimension j, the lower bounds are denoted as x min$j$ and upper bounds are denoted by x max$j$. Here i=1,2,…n,j=1,2,….d.

B. Update Procedure of Adaptive Frequency Modification Velocity and Solution

In BA, a solution is given a randomly generated frequency value, which has the same impact on all of the solution's dimensions. At this stage, the distinctions between a solution's dimensions are pointless. The algorithm's Local Search (LS) performance is decreased by this structure. In contrast, IBA assigns a frequency, which ranges from $fmin$ to $fmax$ to each dimension of a solution independently.

$$diff_j = \sqrt{(x_{ij} - x_j^*)^2}$$

$$range = max(diff) - min(diff) \tag{21}$$

$$\tag{22}$$

$$f_j = f_{min} + \frac{\sqrt{min(diff) - min(diff(j))^2}}{range} * (f_{max} - f_{min})$$

The closest and furthest dimensions of solution i are given as the values fmin and fmax, respectively, after the distances between it and the global best solution are first evaluated for each dimension. Lastly, depending on their distances, the frequencies of the remaining dimensions range between $fmin$ and $fmax$. It should be remembered that a solution's step size is always dependent on frequency. The following updates are required for the velocity formulation:

$$v_{ij}^t = v_{ij}^{t-1} + (x_{ij}^t - x_j^*)f_j \tag{23}$$

C. IBAT for Feature Selection (FS)

The application of the Bat Algorithm to FS is discussed in this section. The subset of features that each bat represents is encoded by its location inside the Search Space (SS). The specifics of the suggested method are detailed in Algorithm 2. The bat population is initialized in the first loop of lines 1–7. Thus, a random binary value corresponding to whether a feature will be selected or not for creating the new dataset is used to initialize the position of the bats. Moreover, in the event that a new solution is approved, the loudness (Ai) and pulse emission rate (ri) are changed. Equations 5 and 6 show that once a bat locates its prey, the Ai normally reduces, but the ri increases.

The values of $f$min and $f$max are set to $fmin$=0 and $fmax$=1. Eventually, the method generates and returns the output vector F containing the chosen features.

Algorithm 2. – FS with IBA

INPUT: Population size m, number of features n, number of iterations T, loudness A, pulse emission rate r, ϵ, α and γ values.

OUTPUT: Subset of features F
1) OF: $f(x), x = x1,\dots xd\ t$
2) Set bat population xi and velocity vi i=1,2 ,..n
3) Delimit pulse frequency fi at xi
4) Set ri and Ai
5) while $t < maximum\ number\ of\ iterations$
6) Create novel solutions via adjusting frequency, and updating velocities and location/solutions.
7) F (rand> ri)
8) Choose a solution among the best solutions
9) Create a local solution around the selected best
10) solution
11) end if
12) if (rand< Ai and $f\ xi < f\ x*$)
13) Accept new solutions

D. Similarity and Indexing Schemes

Images in a database and a QI visual similarity are typically calculated by CBIR systems. The creation of numerous similarity measures for IR based on empirical estimations of feature distribution has been prevalent recently. The retrieval abilities of an IR system would be significantly impacted by various similarity/distance measures. Several frequently used methods for indexing and similarity are covered in this section.

F. Indexing

A major problem in CBIR is effective indexing. Dimension reduction (DR) is typically performed prior to establishing an effective indexing system since image Feature Vectors (FV) are intended to be high dimensional and unsuitable for use in conventional indexing structures. Thus, in order to accomplish this, IBA is used in this instance. The multi-dimensional data are indexed following DR. Indexing is a form of sorting where each image is ranked based on how similar it is to the others. It contributes significantly to the efficient retrieval of image sequences and is helpful in speeding up query performance in the search process [26]. An easy and effective search is aided by proper indexing. The R*-tree method has been suggested in this work to achieve this objective.

R*-tree

The R*-tree shares the similar tree structure with the R-tree, while achieving a better query performance with the application of an enhanced inserting and splitting algorithms for the minimization of overlaps in the leaf nodes [27]. An illustration of an R*-tree is presented in Fig.4.
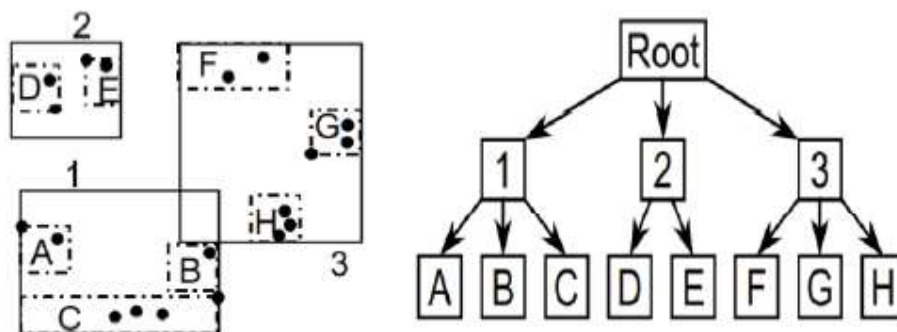
Fig. 5   An image of R*-tree

Relevance Feedback

Image similarity is subjective, task-related, and dependent on substance in the human mind. Generally, content-based approaches can be trusted for IR. Finding meaning in a perceptual or semantic sense is not always guaranteed by retrieval outcomes that rely solely on similarities of visual features.

Additionally, only one part of an image property is attempted to be captured by each feature. In general, users find it challenging to articulate precisely how various elements link together. Interactive relevance feedback, a method utilized in traditional TB information retrieval systems, was created to overcome this problem. One supervised active learning method for increasing information system efficiency is relevance feedback. The concept is to improve system performance by using both positive and negative user examples.

According on predetermined similarity measures, the system retrieves a list of ranked images for a particular query first. The user annotates the obtained images indicating whether they are pertinent (+ve instances) or not (-ve instances) to the query. Based on the user's response, the system will improve the retrieval results and show the user a fresh selection of images. To develop the query and/or modify the similarity measure, the inclusion of both positive and negative instances is therefore the primary concern in relevant feedback.

3.5. Classification

The ordered collection of image classified under a specific heading is called classification. Training and testing are the two processing processes that make up classification. Image features are separated and distinct data is created throughout the training phase. The images are classified using those feature spaces.

3.5.1. Auto-Encoder (AE) based CNN (AE-CNN)

For the purpose of effectively detecting citrus disease, an AE - CNN was presented in this work. As an example, let's consider at a 2-D AE-based CNN with 3 Hidden Layers (HL) in figure 4. Unsupervised learning involves training a (ML) Machine Learning framework F to provide identical outputs to input data x, where $x \approx F(x; w)$, Here, weights of the technique are denoted as w [28]. To minimize the prescribed error function E (such that $w = \text{argminw}[E(x, F(x; w))]$), the ML model F are obtained when w are optimized in this training procedure to minimize E.

The input or output R x is larger in dimension than the internal structure R γ, which is shown by the green parts in Figure 4, which is a noteworthy observation. If the model is effectively trained to provide output that is approximately identical to the input data, then the latent vector γ with low-dimensional has been appropriately localized into the HD data. Finally,

these can be expressed as follows:

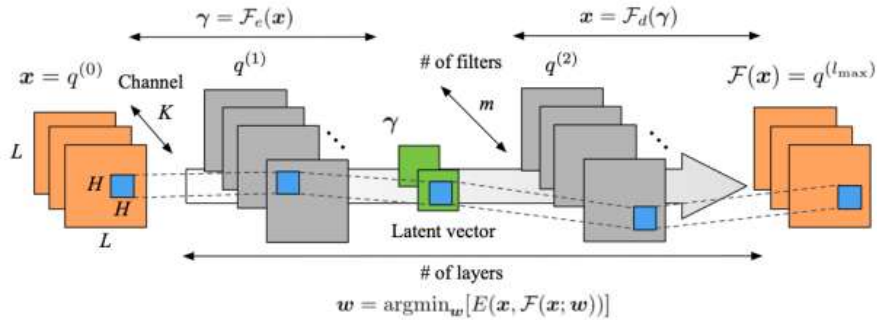$$\gamma = F_e(x), \qquad x \approx F_e(\gamma) \tag{24}$$

Fig. 6   2-D CNN- AE using 3 HL.

The extent of suppressing a dimension strongly relies on the flow field nature and it is illustrated in Fig. 5. Here, the encoder (E) and decoder (D) parts of the AE can be represented as Fe and Fd.

The E in this work is the L2 norm error, and the weights are updated during the iterative training phase using the (AO) Adam Optimizer. The idea of weight sharing has been incorporated throughout CNN training.

At layer l, location (i, j), and filter index m, the CNN node output q (l) is attained in fig 6(a) and (b). This can be attained with the upstream layer q (l−1) output, convolving the filter h (l) (blue H × H squares that is presented in figure 5).

$$q_{ijm}^{(l)} = \varphi(b_m^{(l)} + \sum_{k=0}^{K-1} \sum_{p=0}^{H-1} \sum_{s=0}^{H-1} h_{pskm}^{(l)} q_{i+p-C\ j+s-Ck}^{(l-1)}) \tag{25}$$

Here, an Activation Function (AF), which is often a monotonically increasing NL function is denoted as ϕ, and the values of the parameters C = floor(H/2) that represent the number of flow variables per point for each of the K filters in a Convolution Layer (CL) in the input layer (IL) and Output Layers (OL). ϕ(s) = (e s − e −s) · (e s + e −s) −1 is the hyperbolic tangent function used as the AF in this study.

b (l) m is the bias.

This function was selected after a number of different types of nonlinear AF were examined. Moreover, it was verified that using the sigmoid or ReLU functions in place of the original one would still produce a comparable performance.

Then, the filter coefficients h (l) pskm are optimized as the weights for the purpose of getting a desired output in the CNN training procedure.

A similar network layer's communication of the updated h (l) pskm is shown in Figure 5.

Take note that CNN operates under the assumption that pixels located at great distances from one another do not heavily correlate.

| | 6(a) | 6(b) | 6(c) |
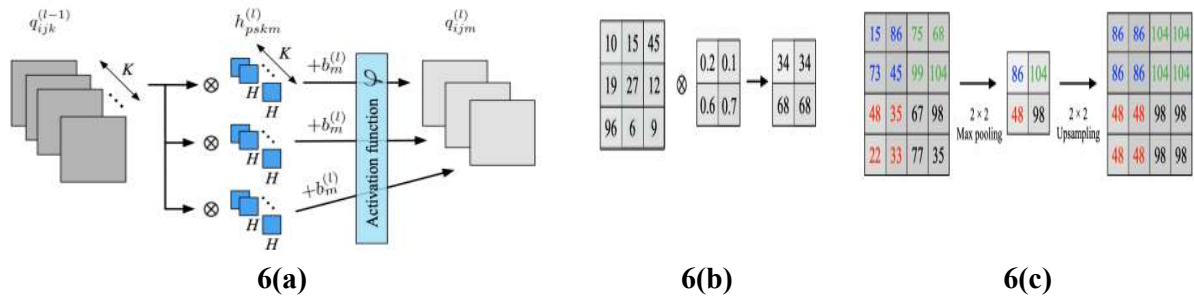
Fig. 7   **Schematics of CNN: (a) the architecture of a single CL; (b) an instance of convolution process; (c) an instance of pooling and upsampling (US) processes.**

Figure 6(c) shows the schematics of the E and Dparts, respectively. To perform DR and dimension extension, and for the E portion, max pooling operation are essential for the development of AE. The AE can obtain resilience against image rotation and translation while reducing the dimension of input images by the max pooling process. By using the nearest neighbor interpolation, the values of the low-dimensional maps are replicated into a high-dimensional (HD) image, via the US procedure in the decoder section. CNN has been used to solve a variety of HD iissues, including fluid dynamics, even though its application in computer science was initially brought forth.

According to reports, the structure of AE-based low-dimensional mapping, which can account for nonlinearities due to the AF, gives it a major edge over linear theory-based techniques.

The reason behind AE-based technique, that are typically lack in interpretability has the following risks: the latent vector that is extracted by NL filter operations and AE-based techniques fails to interpret the latent vector physical meaning. By examining energy containing ratio, the contribution of every latent vector has been interpreted by the researchers and this model does not have concepts like eigen values (EV) or singular values that are found in linear mode decomposition methods. This model is not perpendicular. This type of energy containing ratio was managed by Elman neural network in order to solve this challenge.

3.5.2. Improved Particle Swarm Optimization (IPSO)

To get the optimal solution, PSO employs a large number of particles that move around in the SS as a swarm. Every particle is considered as a point in a D-dimensional space, in accordance with its own flying experience along with the flying experiences of other particles, which modifies its "flying"[29].

To get an optimal solution, the particles travel in D-dimensional space at a certain velocity.

Here, $V_i = (v_{i1}, v_{i2}, \ldots, v_{iD})$ is the expression for the velocity of particle i. $(x, x_{i2}, \ldots, x_{iD})$ represents the location of particle i. Then, ith Particle optimal position, also known as p_{best}, and it is expressed as $p_g = (p_{g1}, p_{g2}, \ldots, p_{gD})$.

Then, g_{best}, the global optimum position of all particles is expressed as $p_g = (p_{g1}, p_{g2}, \ldots, p_{gD})$. To determine the fitness value (FV), each particle in the group has a FF. Equations (26) and (27) in the conventional PSO provide the velocity update formula for dimension d.

$$v_{id} = w \times v_{id} + c_1 \times rand() \times (p_{id} - x_{id}) + c_2 \times Rand() \times (p_{gd} - x_{id}) \qquad (26)$$

$$(X_{id} = x_{id} + v_{id}) \qquad (27)$$

Maximum velocity (vmax), maximum number of iterations (Gmax), acceleration constants C1 and C2, population quantity (Q), inertia weight (w), and the maximum velocity (vmax), and random functions rand () and Rand () with values in [0,1] are among the PSO parameters. Constant 2 is often used as the value for C1 and C2.

In order to overcome the constraints of classical optimization algorithms in handling multiparameter, strong coupling, and nonlinear engineering optimization problems, the IPSO maintains population variety and improves information transfer among populations during optimization. These drawbacks include the propensity to quickly enter local optimization and advanced convergence. The concept of parameter selection for performance is established by analyzing the parameters included in the imported "local-global information sharing" term. Then, in order to confirm the IPSO's global search performance, several sets of classical functions are used to test the performances of the IPSO and classical optimization methods.

This work aims to present an improved IPSO variation that maintains the fast convergence and simplicity of the PSO method while attempting to enhance its performance in finding better solutions. In order to improve the algorithm's capacity for both identifying new regions of the SS that might contain better solutions and taking use of intermediate solutions, a new operation that is both simple and efficient is included into the iterative search process. This is the basis for the distractionfactor (DF). A modified PSO version that is based on parameter settings serves as the foundation for the suggested variant.

Distraction factor

PSO particles will congregate at a certain place when it has not yet found the global optimum, due to the typical of Feature Vectors. In order to ensure the best convergence, distraction factor K was incorporated into PSO. The velocity formula is given in formula (26):

$$v_{id} = K[v_{id} + c_1 \times rand() \times (p_{id} - x_{id}) + c_2 \times Rand() \times (p_{gd} - x_{id})] \qquad (28)$$

The suggested formula for calculating the distraction factor K was applied in this work via Algorithm.1. In Clerc's experiment, values c1 and c2 both used 2.05, the same value. For this experiment, set aside four decimal places for K. The particular velocity formula is found in formula (5):

$$v_{id} = 0.7298 \times [v_{id} + 2.05 \times rand() \times (p_{id} - x_{id}) \qquad (29)$$
$$+ 2.05 \times Rand() \times (p_{gd} - x_{id})$$

To find the optimal solution's expected position in the early rounds of PSO, a particle must detect throughout a large range. To find the optimal point in subsequent rounds, it must evolve locally within a small range. As a result, K ought to take a lower value later on and a bigger value early on. During a prolonged late stage period, K should gradually drop to the minimum. The con-cave function is consistent with this pattern of change.

To allow the particles to find the best solution over a wide range, the distraction factor should select a convex function in the early iterations to prevent premature convergence. In order to allow for the slow development of the DF to the minimum in the late phase, it should select a concave function. It guarantees that the method will converge. In accordance with this concept, formula (30) illustrates the functional DF structuring based on the cosine function:

$$K = \frac{\cos((\pi/G_{max}) \times T) + 2.5}{4} \qquad (30)$$

Here, the iteration count is T. The changing value K curve appeared when Gmax= 40. K's curve in the function is first a convex function and eventually becomes a concave function. Formula (26) becomes formula (31) after the value K is substituted in (26). The following describes formula (31):

$$v_{id} = \left(\frac{\cos((\pi \times T/G_{max})) \times 2.5}{4} \right) \times [v_{id} + 2 \times rand() \times (p_{id} - x_{id}) \qquad (31)$$
$$+ 2 \times Rand() \times (p_{gd} - x_{id})]$$

Algorithm 3. IPSO

Input : Input data
Output: Optimized features
For every particle i
For every dimension d
      Set location x_{id} arbitrarily in permitted range
      Set velocity v_{id} arbitrarily in permitted range
End For
End For
Iteration k=1
Do
While iter$_{max}$ is not attained or minimum error criterion is not met do
For every particle do
      Compute the FV;
      If the FV is better than the best FV in history (pbest)
      Fix current value as the new pbest;
End
End
For every particle do
Determine the particle neighborhood the particle using the best fitness (gbest);
Choose randomly a velocity for the particle (V$_{p-ran}$);
Compute particle velocity v_{pj}^i according to eq.(26)
Compute the particle position p_{pj}^i
Implement K by eq (30)
Update every particle position and velocity
Calculate all population
End

4. Results and Discussion

The IBSR dataset (http://www.cma.mgh.harvard.edu/ibsr/), which contains multiple scan images of individuals with and without BT, is the subject of this discussion, which examines the experimental results from three algorithms. It is considered that the query judgment is defined on the image categories in order to have an objective performance measure [22]. The average ratio of the total number of returned images to the number of relevant images is an evaluation metric, which is simply called Average Precision. Assuming that the user's query target is a category, the experiments begin with a random selection of categories from the database. By using relevance feedbacks, the system then improves the retrieval outcomes. Using the ground truth database, ten instances are selected at random and labeled as positive or negative for each iteration of the relevance feedback process.

The tests assessed the efficiency of several approaches in the detection of ASD data by

utilizing multiple criteria that are commonly utilized in BC. To compute various performance metrics, first measure the true positive (TP), false positive (FP), true negative (TN), and false negative (FN) rates. Precision, which is the percentage of retrieved instances that were relevant, was the first performance metric. The percentage of pertinent instances that were retrieved was known as recall, and it was the second performance metric. The measurements of precision and recall are crucial for assessing a prediction approach's performance, even if they are frequently conflicting.

In order to create a single metric, the F-measure, these two measurements can be merged with equal weights. Accuracy, which is the percentage of accurately predicted instances to all predicted instances, was the last performance metrics to be calculated.

By dividing the correctly predicted positive observations to the overall predicted positive observations, the precision is calculated.

$$Precision = TP/(TP + FP) \tag{32}$$

By dividing the correctly predicted positive observations to the overall observations, the Sensitivity or recall is calculated.

$$Recall = TP/(TP + FN) \tag{33}$$

The F-measure is the weighted average of recall and precision. It require both FP and FN.

$$F - measure = 2 * (Recall * Precision)/(Recall + Precision) \tag{34}$$

Accuracy is calculated using both positive and negative.

$$Accuracy = (TP + FP)/(TP + TN + FP + FN) \tag{35}$$

By the parameters sensitivity and specificity, the ratio of accurately diagnosed tumor pixels to non-tumor pixels is determined. Accuracy is defined as the ratio of all correctly identified tumor pixels
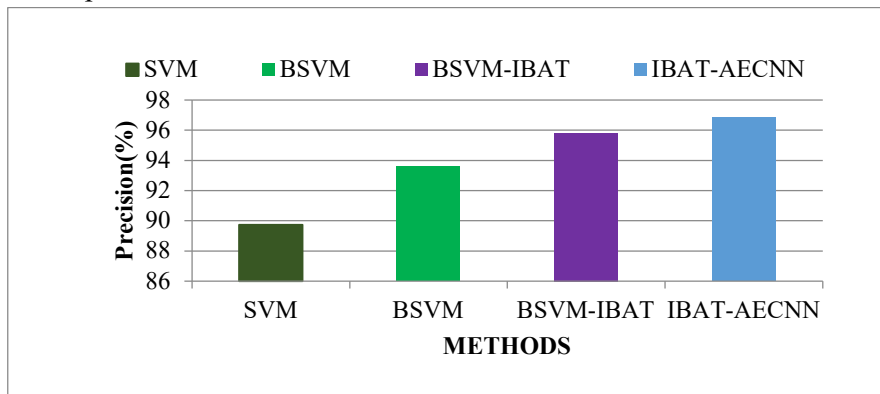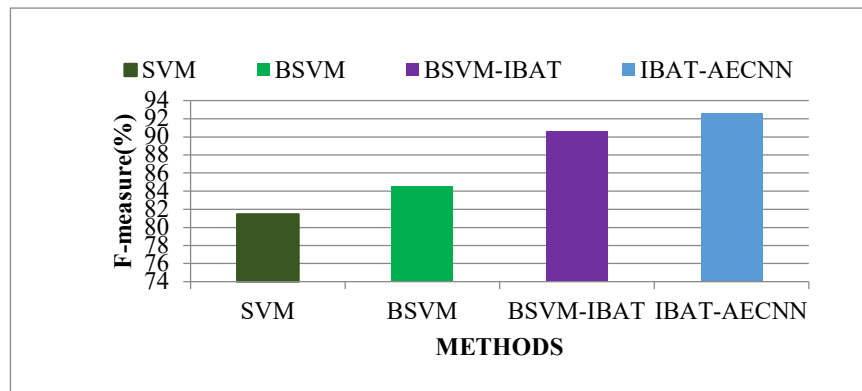

Fig. 8   Precision comparison outcomes of the suggested and current approaches

Figure 7 presents the precision comparison performance of the suggested and current approaches. Consequently, the outcomes confirm that BT classification may be accurately predicted using FE utilizing HFDSO. Therefore, there are a lot of beneficial features in the suggested HFDSO that fail to significantly impact linear transformation performance. This is a desirable feature since it eliminates the need for tedious regularization parameter tuning in the classifier. The classification issue can be addressed with great effectiveness by using the method suggested by the HFDSO.
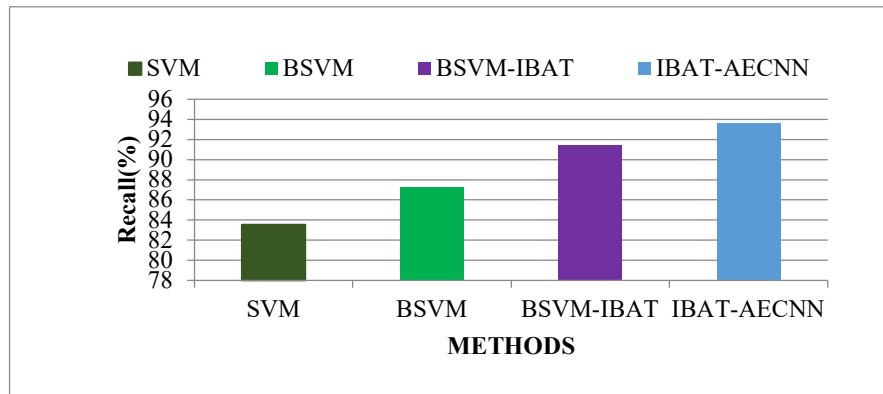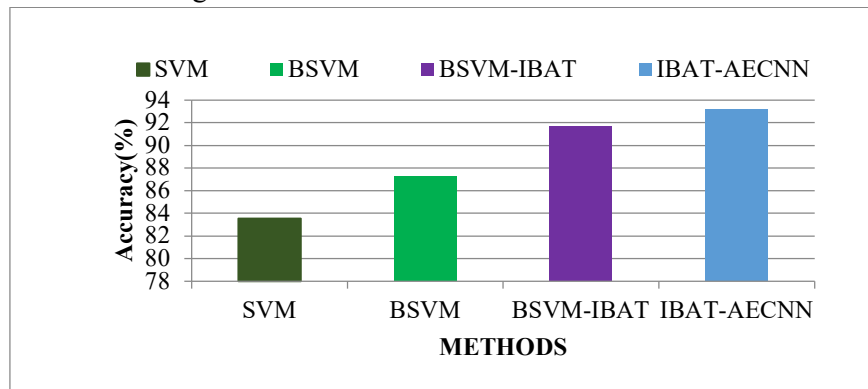
Fig. 9   **Recall comparison outcomes of the suggested and current approaches**

The performance results of the suggested and current procedures are shown in figure.8. The findings therefore indicate that, in comparison to the current technique, which delivers lower recall results, the BSVM-IBAT method metric has 91.74, the BSVM method has 89.68%, and the SVM method metric has 87.25%, the suggested method delivers high recall outcomes of 93.62%.

Fig. 10   **F-measure comparison outcomes of the suggested and current approaches**

In comparison to the BSVM-IBAT, BSVM, and SVM, the suggested AE based CNN performs well in terms of the disease prediction rate, as seen in figure 9. ML-based qualitative analysis and quantitative analysis delivers results that agree with each other in terms of F-measure. Regarding accuracy for the specified dataset, the suggested HFDSO is contrasted with otherSOTA classification algorithms.

Fig. 11   **Accuracy comparison outcomes of the suggested and current approaches**

The suggested approach outperforms the current classifier in terms of accuracy, as seen

in Figure 10. Comparatively, when applied to static data, all of the previously stated classifiers perform poorly in comparison to the IBAT-AECNN classifier, demonstrating the method's efficacy in all crucial scenarios for the classification of BT. When compared to other classifiers constructed on previously developed models, the accuracy of the classifiers will be higher.

5. Conclusion

In the medical field, CBVIR undoubtedly has a lot of potential. The volume of visual data generated in medical departments highlights the need for novel and alternate access strategies to supplement textual information. Applications for content-based approaches are numerous and include a wide range of images. This paper offers a two-level hierarchical CBMIR system that finds the most comparable images within the identified class after first classifying the QI of a BT as benign or malignant. During the image preprocessing step, NR and image normalization are completed. Following this stage, the hybrid fuzzy DSOA is used for FE and image segmentation utilizing the WS method to identify the tumor part in the MRI image. The Mbat algorithm is then used to carry out FS. In the end, a CNN is suggested as an effective method of BT diagnosis. Brain MRI data from MI database have been used in experiments. By increasing precision, recall, and retrieval time, the suggested method produces good retrieval outcomes. For better performance, the features were applied to tested classifier models. The method had the highest classification accuracy when compared to all relevant works.

References

1. Müller, H., Michoux, N., Bandon, D., & Geissbuhler, A. (2004). A review of content-based image retrieval systems in medical applications—clinical benefits and future directions. *International journal of medical informatics*, *73*(1), 1-23.
2. Mitra, S., & Shankar, B. U. (2015). Medical image analysis for cancer management in natural computing framework. *Information Sciences*, *306*, 111-131.
3. Bauer, S., Wiest, R., Nolte, L. P., & Reyes, M. (2013). A survey of MRI-based medical image analysis for brain tumor studies. *Physics in Medicine & Biology*, *58*(13), R97.
4. Siggelkow, S. (2002). *Feature histograms for content-based image retrieval* (Doctoral dissertation, Freiburg (Breisgau), Univ., Diss., 2002).
5. Habiba, S. U., Islam, M. K., Nahar, L., Tasnim, F., Hossain, M. S., & Andersson, K. (2022, October). Brain-DeepNet: a deep learning-based classifier for brain tumor detection and classification. In *International Conference on Intelligent Computing & Optimization* (pp. 550-560). Cham: Springer International Publishing.
6. Zacharaki, E. I., Wang, S., Chawla, S., Soo Yoo, D., Wolf, R., Melhem, E. R., & Davatzikos, C. (2009). Classification of brain tumor type and grade using MRI texture and shape in a machine learning scheme. *Magnetic Resonance in Medicine: An Official Journal of the International Society for Magnetic Resonance in Medicine*, *62*(6), 1609-1618.
7. Çınar, N., Kaya, B., & Kaya, M. (2022, March). Comparison of deep learning models for brain tumor classification using MRI images. In *2022 International conference on decision aid sciences and applications (DASA)* (pp. 1382-1385). IEEE.

8. Badjie, B., & Ülker, E. D. (2022). A deep transfer learning-based architecture for brain tumor classification using MR images. *Information Technology and Control*, *51*(2), 332-344.

9. Mandle, A. K., Sahu, S. P., & Gupta, G. P. (2022). CNN-based deep learning technique for the brain tumor identification and classification in MRI images. *International Journal of Software Science and Computational Intelligence (IJSSCI)*, *14*(1), 1-20.

10. Qodri, K. N., Soesanti, I., & Nugroho, H. A. (2021). Image analysis for MRI-based brain tumor classification using deep learning. *IJITEE (International Journal of Information Technology and Electrical Engineering)*, *5*(1), 21-28.

11. Remzan, N., Tahiry, K., & Farchi, A. (2022). Brain tumor classification in magnetic resonance imaging images using convolutional neural network. *IJECE*, *12*(6), 6664.

12. Deepak, S., & Ameer, P. M. (2019). Brain tumor classification using deep CNN features via transfer learning. *Computers in biology and medicine*, *111*, 103345.

13. Dubey, S. R., Singh, S. K., & Singh, R. K. (2015). Local wavelet pattern: a new feature descriptor for image retrieval in medical CT databases. *IEEE Transactions on Image Processing*, *24*(12), 5892-5903.

14. Aljohani, M., Bahgat, W. M., Balaha, H. M., AbdulAzeem, Y., El-Abd, M., Badawy, M., & Elhosseini, M. A. (2024). An automated metaheuristic-optimized approach for diagnosing and classifying brain tumors based on a convolutional neural network. *Results in Engineering*, *23*, 102459.

15. Balamurugan, T., & Gnanamanoharan, E. (2023). Brain tumor classification in MRI images using genetic algorithm appended CNN. *Computer Assisted Methods in Engineering and Science*, *30*(3), 305-321.

16. Gómez-Guzmán, M. A., Jiménez-Beristaín, L., García-Guerrero, E. E., López-Bonilla, O. R., Tamayo-Perez, U. J., Esqueda-Elizondo, J. J., ... & Inzunza-González, E. (2023). Classifying brain tumors on magnetic resonance imaging by using convolutional neural networks. *Electronics*, *12*(4), 955.

17. Rasheed, Z., Ma, Y. K., Ullah, I., Al Shloul, T., Tufail, A. B., Ghadi, Y. Y., ... & Mohamed, H. G. (2023). Automated classification of brain tumors from magnetic resonance imaging using deep learning. *Brain Sciences*, *13*(4), 602.

18. AlTahhan, F. E., Khouqeer, G. A., Saadi, S., Elgarayhi, A., & Sallah, M. (2023). Refined automatic brain tumor classification using hybrid convolutional neural networks for mri scans. *Diagnostics*, *13*(5), 864.

19. Wu, M., Liu, Q., Yan, C., & Sen, G. (2023). Multi-Classification of brain tumors on magnetic resonance images using an ensemble of pre-trained convolutional neural networks. *Current Medical Imaging*, *19*(1), 65-76.

20. Muhammad, L. J., Badi, I., Haruna, A. A., Mohammed, I. A., & Dada, O. S. (2022). Deep learning models for classification of brain tumor with magnetic resonance imaging images dataset. In *Computational Intelligence in Oncology: Applications in Diagnosis, Prognosis and Therapeutics of Cancers* (pp. 159-176). Singapore: Springer Singapore.

21. Gull, S., Akbar, S., & Naqi, S. M. (2023). A deep learning approach for multi-stage classification of brain tumor through magnetic resonance images. *International Journal of Imaging Systems and Technology*, *33*(5), 1745-1766.

22. Rastogi, D., Johri, P., Tiwari, V., & Elngar, A. A. (2024). Multi-class classification of brain tumour magnetic resonance images using multi-branch network with inception block and five-fold cross validation deep learning framework. *Biomedical Signal Processing and Control*, *88*, 105602.

23. Guruvasuki. R, Josephine Pushpa Arasi. A, 2013, "MRI Brain Image Retrieval Using Multi Support Vector Machine Classifier", International Journal of Advanced Information Science and Technology, Vol.10, Pp No. 29-36

24. Zhang B, Shan S, Chen X, Gao W., 2007," Histogram of Gabor Phase Patterns (HGPP)", A Novel Object Representation Approach for Face Recognition. IEEE Trans Image Process. 16(1):57–68.

25. Su, M. C., Chen, J. H., Utami, A. M., Lin, S. C., & Wei, H. H. (2022). Dove swarm optimization algorithm. *IEEE Access*, *10*, 46690-46696.

26. Sunitha Jeyasekhar, Sihem Mostefai, "Towards Effective Relevance FeedBack Methods in Content-Based Image Retrieval Systems," In Proceedings of the 2nd International Conference on Information and Multimedia Technology.

27. Bechmann, N, Kriegel, H, Schneider, R. And Seeger, B. 1990, "The R* tree: An efficient and robust access method for points and rectangles", Proceedings of the SIGMOD, pp. 322–332.

28. Gu, J., Wang, Z., Kuen, J., Ma, L., Shahroudy, A., Shuai, B., ... & Chen, T. (2018). Recent advances in convolutional neural networks. *Pattern recognition*, *77*, 354-377.

29. Wang, D., Tan, D., & Liu, L. (2018). Particle swarm optimization algorithm: an overview. *Soft computing*, *22*(2), 387-408.